Dark current spikes as an indicator of mobile dislocation dynamics under intense dc electric fields

Eliyahu Zvi Engelberg,[1] Jan Paszkiewicz,[2] Ruth Peacock,[2] Sagy Lachmann,[1] Yinon Ashkenazy,[1,*] and Walter Wuensch[2]

[1]*Racah Institute of Physics and the Center of Nanoscience and Nanotechnology, The Hebrew University of Jerusalem, Jerusalem 9190401, Israel*

[2]*CERN, CH-1211 Geneva-23, Switzerland*

(Received 28 June 2020; accepted 2 December 2020; published 17 December 2020)

Breakdown of metals subject to intense electric fields is a long-standing limiting factor in high-voltage applications. The mechanism leading to breakdown nucleation is not completely understood. Previously, it was suggested that breakdown can be nucleated by a critical transition in the population of mobile dislocations near the surface of electrodes. This was formulated in terms of a mean-field mobile dislocation density fluctuation (MDDF) model. Based on this model, it was proposed that prebreakdown fluctuations of the mobile dislocation density might be observed as spikes in the dark current between the electrodes. We constructed a setup in which these fluctuations were measured. The rate of fluctuations, as a function of the electric field between the electrodes, agrees with the predictions of the MDDF model, both in functional form and in absolute numerical rates. This numerical agreement was obtained using previously derived numerical parameters of the model. In addition, for each electric field, the distribution of times between current fluctuations was examined. The results indicate that each such prebreakdown fluctuation is the result of a two-step process. This characteristic, too, is in line with the MDDF model, which predicts that a characteristic prebreakdown current event is described as two separate steps in a Markov process, occurring in quick succession.

DOI: 10.1103/PhysRevAccelBeams.23.123501

I. INTRODUCTION

A. Vacuum breakdown

High-gradient technologies rely on the maintenance of high voltages between metallic electrodes. In systems sustaining such high voltages, plasma originating from the electrodes can effect an electrical discharge between them. This is called *vacuum arcing*, or *vacuum breakdown*, and is a long-standing problem in high-voltage applications, limiting the obtainable amplitudes of electric and electromagnetic fields [1–4].

The development of quantum mechanics led to the recognition that field emission, in which electrons are released from the electrodes due to the electric field, is a necessary step in the nucleation of vacuum breakdown [5]. However, the precise mechanism leading to breakdown nucleation is not yet understood. This problem has assumed importance due to the initiation of next-generation linear collider projects, which employ strong radio frequency (rf) electromagnetic fields. In each of these, breakdown has become a limiting factor [6]. An improved understanding of breakdown would be valuable for other fields in which breakdown is relevant, too, as either a desired effect or one to be prevented.

One linear collider project, in which understanding and controlling breakdown are pivotal topics, is the prospect study for the compact linear collider (CLIC) in CERN. CLIC aims to produce rf accelerating gradients of up to 100 MV/m, which will be used to collide a beam of electrons with a beam of positrons. These rf fields are to be produced in pulses of about 200 ns each at a repetition rate of 50 Hz. At the initial stage, in which the length of the linac will be 11.4 km, the collision energy will reach 380 GeV. The present goal at CLIC is to reduce the breakdown rates to 3×10^{-7} breakdowns per pulse per meter (bpp/m) of accelerator length [7].

To investigate breakdowns in an environment which is simpler, and more specifically targeted to their study, direct current (dc) setups were constructed in CERN and elsewhere. One of these is the large electrodes system (LES) in CERN, in which the experiment to be described in this manuscript was conducted. While some characteristics of

*yinon.ash@mail.huji.ac.il

the rf and dc setups obviously differ, many insights gained from dc measurements were shown to be valid in rf systems, too [8–10].

B. The MDDF model

Surface features have been postulated to be essential in the development of breakdown [11–13]. However, after an initial state of conditioning, breakdown rates normally saturate at an approximately constant level [14,15]. This suggests that breakdown sites are intrinsic and formed during operation, since preexisting surface formations or extrinsic sources would be depleted over time. In addition, prebreakdown surface features have not been observed experimentally [3,11,12,16].

We previously proposed [17,18] that a critical transition in the density of the mobile dislocations within a metal can lead to a rapid increase in local current. This mobile dislocation density fluctuation (MDDF) model provides a description of the initial stage of breakdown nucleation, showing that intense electric fields can cause surface response, thus nucleating breakdown [17,18]. This description is in line with previous suggestions that the electric field and current are enhanced due to the formation of a protrusion, leading to localized heating and plasma formation through evaporation [16,19], and thus to breakdown [1,20,21]. However, in the MDDF model, the localized plastic activity leading to this enhancement is the result of a rapid transition in the mobile dislocation population, which does not produce observable features prior to breakdown. In addition to providing a qualitative explanation of the characteristics of breakdown nucleation, the MDDF model also provides statistical tools to calculate breakdown rates, which are in agreement with experimental observations [17,18,22,23].

C. Dark current fluctuations

The surface of a metal serves as a potential barrier for its conduction electrons. These electrons can be released by tunneling through the barrier. When a strong electric field is applied to the surface of the metal, *field emission* occurs, in which the amount of electrons released increases rapidly as a function of the field. This creates a *dark current* between electrodes in high-gradient setups, which was recognized as a probable precursor of breakdown. It was further recognized that the electric field might be enhanced at certain locations on electrode surfaces, due to their deformation [24].

In order to investigate this field enhancement, experiments were conducted in which the average dark current was measured in high-gradient setups. The results were then compared to theoretical predictions of the tunneling rate, which took into account possible deformations of the electrode surfaces. This allowed the estimation of the field enhancement factor, which is the amount by which an applied field is increased to a local microscopic value. Typically, the field enhancement factor was found to have values ranging between 40 and 100 [8,24–26].

As described above, the prebreakdown surface features which would lead to the existence of such field enhancement factors have not been observed, and, in the MDDF model, are not predicted to exist prior to breakdown. However, according to the model, subcritical fluctuations of the mobile dislocation density might be observed as *fluctuations* of the dark current during routine operation [17,18]. For a study of these fluctuations, a measurement of the changes in the dark current, rather than its average value, are necessary. Such measurements have now been carried out at CERN in a dedicated system, and the purpose of this manuscript is to compare their results to the time distribution of fluctuations derived from the MDDF model.

In a previous study, four physical parameters, which were not determined *a priori*, were estimated by carrying out a least squares fit to various measurement sets of breakdown rates as a function of the electric field and temperature [17,18]. Here we demonstrate that the MDDF model, with the same values of parameters obtained from that fit, reproduces the observed dark current fluctuation rates.

The rest of this manuscript is organized as follows: The experimental setup is described in Sec. II, and the resulting measurements are presented in Sec. III. In Sec. IV, the MDDF model is applied to calculate the dark current fluctuation rates, and the resulting predictions are shown to agree with the measurements. Finally, in Sec. V we suggest that this apparent link between dark current fluctuations and breakdown rates can be utilized to improve operational procedures in high voltage setups. We also propose additional experiments, which can further validate the MDDF model and its link to dark current fluctuations.

II. EXPERIMENTAL SETUP

Measurements of prebreakdown dark currents were performed in the large electrode system (LES) at CERN. The LES is designed to test various electrodes under high-gradient conditions, enabling application of electric fields up to ~100 MV/m, in vacuum levels in the range of 1 pbar (see [9,10] for a detailed description). Here we used oxygen-free high conductivity (OFHC) Cu electrodes (grain diameter ~1 mm, Ra0.025). Each such electrode was shaped as a cylinder with a diameter of 80 mm, with a circular protrusion of 60 mm diameter from the shoulder. The center of each such protrusion, facing the opposite electrode, featured a machined 10 mm × 1 mm rectangular ridge. A ceramic was placed between the shoulders of the electrodes to maintain a gap of 60 μm between the ridges. These ridges were initially arranged crosswise, giving about 1 mm^2 area exposed to the high field, and then rotated to be parallel, increasing the area to 10 mm^2 (see Fig. 1). The conditioning process allowed these ridged electrodes to sustain fields of up to 60 MV/m. (This is lower than the typically achieved level in the LES [10],

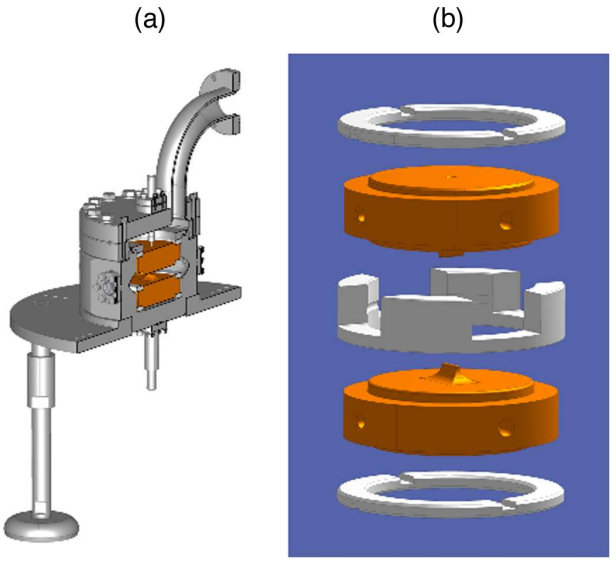

FIG. 1. (a) Sketch of the LES vacuum chamber and (b) detail of the mechanical assembly, holding crossed ridged electrodes.

possibly due to the altered shape of the electrodes.) Applied voltages were limited by this maximum sustainable field, as well as the maximum 1 mA obtainable current.

The electric field between the electrodes can be estimated as $E = V/d$, where V is the applied voltage, and d is the distance between their ridges [9]. A more detailed estimate can be achieved by simulation. Figure 2 shows the electric field on a plane adjacent to the surface of one of the electrodes, in the vicinity of the area between the ridges, for crossed and parallel ridges. The results in the figure were obtained using CST STUDIO SUITE. The total measured capacitance of the system, when the ridges were parallel, was 87 pF, so the energy stored in the system for, e.g., a voltage of 3 kV, can be estimated as 392 μJ.

A specialized electric setup, shown in Fig. 3, was used to search for the subcritical fluctuations predicted by the MDDF model. The signal output is capacitively coupled to

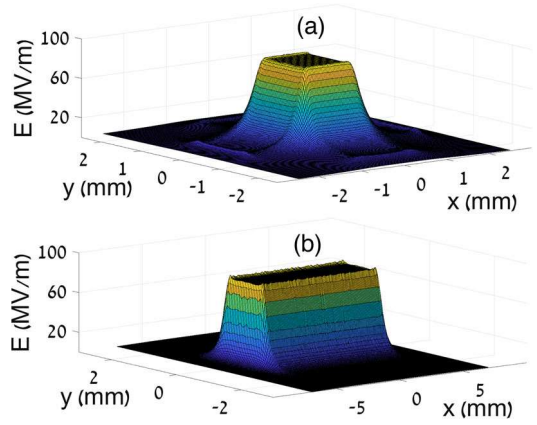

FIG. 2. Electric field adjacent to an electrode surface, in the vicinity of its ridge, for (a) crossed and (b) parallel electrodes. The applied voltage is 5 kV.

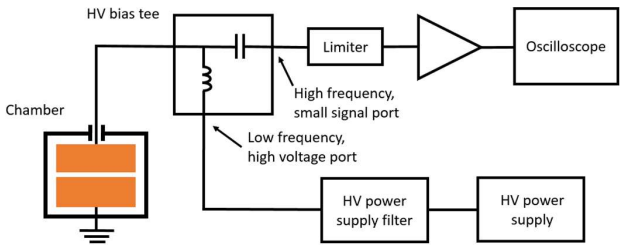

FIG. 3. Block diagram of the setup used to measure dark current fluctuations.

the high-voltage line, followed by input protection and low-noise amplifiers, before being sampled by an oscilloscope, with 1 μA of dark current corresponding to approximately 1.75 mV measured by the oscilloscope. The system was designed for a broad bandwidth (>1.5 GHz) and low noise, to account for as large a range of signals as possible, since the characteristics of the signal were not known *a priori*. A power supply filter was added to attenuate any residual electrical noise from the switching behavior of the high-voltage power supply.

In both configurations, measurements of the dark current as a function of time showed pronounced brief current spikes occurring at varying intervals. These unique subcritical prebreakdown events, see, e.g., Fig. 4, consist of a fast transient of ~50 ns followed by a decaying sinusoid at ~2.5 MHz. The latter is thought to be the resonant response of the setup to the initial current spike. Measurements are performed via capacitive coupling, resulting in a high-pass response which removes the dc component of the dark current. This precludes the differentiation among transient spikes and step changes in the dark current. For obtaining a statistically significant amount of events, a low sampling rate of 5 MHz was used, thus optimizing oscilloscope memory usage (and avoiding the need to process prohibitively large amounts of data). Although this rendered the initial spike too fast to resolve, the 2.5 MHz ringing remained visible, thus allowing to determine the time of occurrence per spike and their ensuing time distribution, which is the focus of this study.

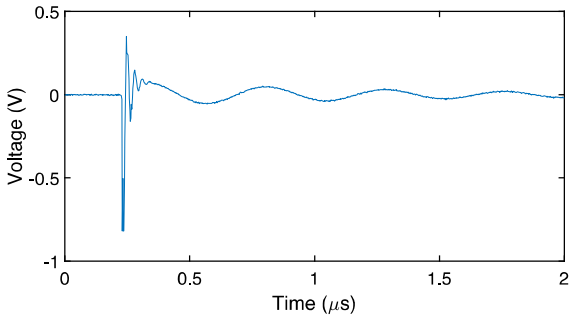

FIG. 4. Example oscilloscope trace of a subcritical (i.e., prebreakdown) current spike, recorded at a high sample rate of 500 MHz.

TABLE I. List of measurement series.

Series	Electrode configuration	Symbol in Fig. 7	β
A	Crossed	Circles	3.2
B	Crossed	Diamonds	1.8
C	Parallel	Triangles	1.7
D	Parallel	Squares	0.5
E	Parallel	x	0.6

III. RESULTS

Five series of measurements, as listed in Table I, were performed. Over the course of each series, the applied voltage was varied in steps. An algorithm was applied to assign a time of occurrence to each current spike, avoiding double counting due to the ringing. Using this algorithm the distribution of time intervals between the spikes, for each voltage in each measurement series, was calculated. The cumulative distribution function (CDF) and frequency histogram of these distributions, for a few example voltages in one series, are shown in Figs. 5 and 6, respectively.

For further details of the course of each measurement series and the algorithm used to identify the spikes, see the Appendixes A and B.

Each measured distribution was characterized by an average rate of occurrence of spikes r_s. This rate as a function of the electric field E, for every measurement series, is shown in Fig. 7. (Here $E = V/d$, as described in Sec. II. The field at the surface of the electrodes can have a different value, due to their shape and surface deformation. This difference is incorporated in the parameter β, see Sec. IV and Refs. [17,18]). The rates in Fig. 7 are given in units of spikes per second per slip plane, under the assumption that an active slip plane can develop in an area of approximately $\Delta\rho^{-2} = 10^{-4}$ mm^2 [18].

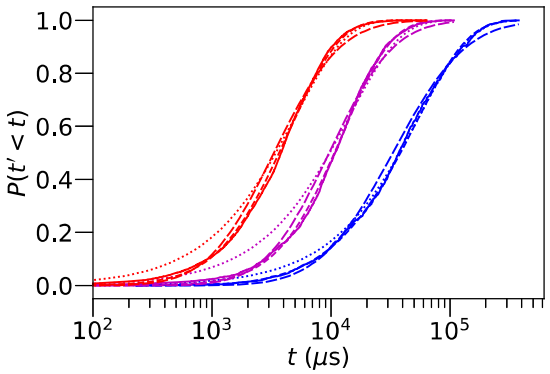

FIG. 5. CDF of the time interval between current spikes for electric fields of 31.3, 35.4, and 39.6 MV/m (from right to left), from series D. For each field, the CDF calculated from experiment is drawn as a solid line. The other lines represent best fits to hypoexponential (dashed), exponential (dotted), and log-normal (dash-dotted) distributions.

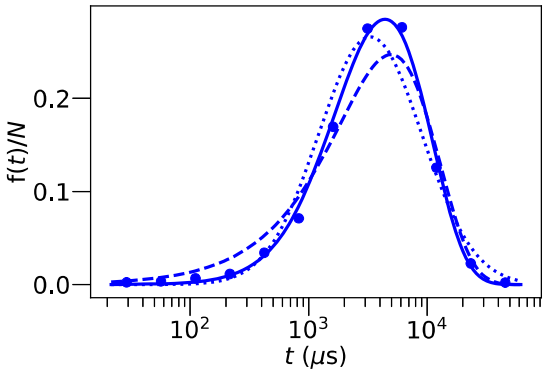

FIG. 6. Histogram of the time interval between current spikes for an electric field of 39.6 MV/m, from series D. The time intervals are divided logarithmically into thirteen bins, and the frequency axis is normalized by the total number of samples. The circles represent the experimental results (with error bars that are smaller than the size of the symbols), and the lines represent best fits to hypoexponential (solid), exponential (dashed), and log-normal (dotted) distributions. The logarithms of the likelihood ratios are $\ln(L_h/L_e) = 227$ for the hypoexponential and exponential fits, and $\ln(L_h/L_l) = 466$ for the hypoexponential and log-normal fits.

As seen in Fig. 7, spikes were observed at fields starting from a threshold field E_{th}, varying between 21 and 29 MV/m among series, and r_s was found to be an increasing function of $E - E_{\text{th}}$. However, as progressing series of measurements were made, this dependence became milder, and the overall values of r_s decreased. This decrease over time is in line with the proposal that the current spikes are connected to the breakdown rate, since high-voltage electrodes are known to undergo a conditioning process, in which exposure to strong electromagnetic fields over time makes them less susceptible to subsequent breakdown [9,10,22]. The electric field and vacuum were retained between series, so that the electrodes were

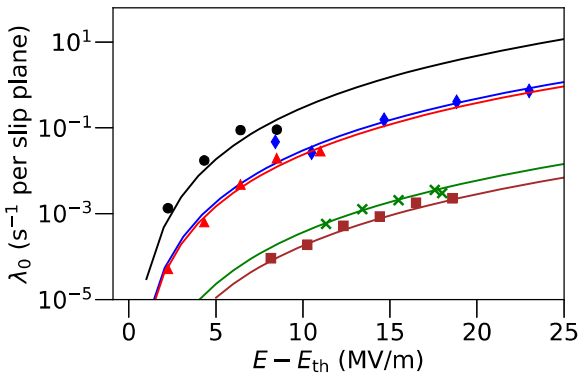

FIG. 7. Rate of current spikes as a function of the electric field, experimental (markers, whose size also accounts for experimental error) and theoretical (lines), for the measurement series listed in Table I. The theoretical lines differ only in the parameter β, as detailed in the table.

continuously being conditioned between them. This long-term conditioning mechanism does not preclude short-term deviations, as observed between series D and E. Indeed, short-term increases of the breakdown rate as a function of the electric field are regularly observed in the conditioning process.

IV. COMPARISON TO THEORY

A. Theoretical interpretation of current spikes

It was proposed in [18] that fluctuations of the mobile dislocation density within slip planes of a metal, subjected to a strong electric field, can be described as a birth-death Markov process. In this process the density n, representing the number of mobile dislocations in one slip plane, can change by ± 1, normally fluctuating around $n_* = 0$, and ranging from 0 to a critical density n_c. When n reaches n_c a critical transition occurs, leading to a runaway increase in n and, subsequently, to possible breakdown nucleation [17,18].

The corresponding birth and death rates of the Markov process are

$$\lambda_n = \frac{25\kappa C_t c}{G^2 b \Delta\rho}\sigma^2 e^{-\frac{E_a-\Omega\sigma}{k_B T}}; \qquad \mu_n = \frac{50\xi C_t c}{G}\sigma n. \tag{1}$$

Here σ is the stress in the slip plane, given by $\sigma = \epsilon_0(\beta E)^2/2 + ZGb\Delta\rho n$, T is the temperature, and E is the electric field. The rest of the constants, listed in Table II, are physical values obtained by microscopy, *a priori* physical considerations, and fitting the MDDF theory to measured breakdown rates. It was shown that the variation among experimental structures of the breakdown rates, as a function of the electric field, can be explained as a difference in only one parameter, β [18].

The breakdown rate is clearly not equal to r_s, since the latter is the rate of a prebreakdown phenomenon. To estimate r_s we consider that, prior to breakdown, each active slip-plane system is in a metastable state, in which the creation and arrest of mobile dislocations occur regularly. An increase in the density of mobile dislocations, in cells on the surface of the cathode, can be expected to modify the surface structure. This, in turn, may affect the dark current between the electrodes. We therefore consider the possibility that the spikes of dark current can be described in terms of the same kinetic model as that of the breakdown rate.

To analyze this hypothesis quantitatively, we consider an increase in mobile dislocations, i.e., a transition from any state n to the state $n+1$. The rate of such a transition is given by $\pi_n\lambda_n$, where π_n is the value of the quasistatic distribution function (see [17,18]) at n. In the range of interest for experimental setups, $\lambda_0 \gg \lambda_{n>0}$, and also $\pi_0 \approx 1 \gg \pi_{n>0}$. The rate at which birth events occur is, therefore, approximately equal to λ_0. In addition, since in the experimental range of interest we have $\mu_{n+1} \gg \lambda_n$ for every n (and in particular $\mu_1 \gg \lambda_0$), practically every birth event will be closely followed by a death event. λ_0 can be thought of, then, as the rate at which dark current spikes, each representing a birth-and-death pair of events, will occur. Therefore, λ_0 can be used to approximate r_s.

TABLE II. Constants and fitted parameters of the MDDF model [18].

Symbol	Value	Meaning
κ	0.32	Kinetic factor of dislocation creation[a,b]
C_t	2.31 km/s	Velocity of sound in Cu
c	1 μm^{-1}	Density of barriers in slip plane[c]
G	48 GPa	Shear modulus in Cu
b	0.25 nm	Burgers vector in Cu
$\Delta\rho$	0.1 μm^{-1}	Discrete change in mobile dislocation density[c,d]
E_a	0.8 eV	Activation energy of dislocation creation[b]
Ω	5.6 eV/GPa	Activation volume of dislocation creation[b]
k_B	86.2 μeV/K	Boltzmann constant
ξ	1	Mobile dislocation trap efficiency
ϵ_0	8.85 pF/m	Permittivity of vacuum
β	4.6	Stress/field enhancement factor[e]
Z	1	Structural parameter[f]

[a]Dependent on the activation entropy of the dislocation sources.
[b]Fitted to observed breakdown rates.
[c]Observed by microscopy.
[d]Inverse of dislocation cell size.
[e]Fitted value for the reference data set of breakdown rate measurements. This value is varied to account for the diversity of results among measurements in different structures.
[f]Linking stress to mobile dislocation density.

B. Dependence on the electric field

From Eq. (1), we find that

$$\lambda_0 = \frac{25\kappa C_t c}{G^2 b \Delta\rho}\sigma_0^2 \exp\left(-\frac{E_a - \Omega\sigma_0}{k_B T}\right). \tag{2}$$

Here, we might expect $\sigma_0 = \sigma(n=0) = \epsilon_0(\beta E)^2/2$. However, we saw in the experiment that current fluctuations occur only above E_{th}. This observation leads us to redefine the effective stress for mobile dislocation nucleation as

$$\sigma_0 = \frac{1}{2}\epsilon_0[\beta(E - E_{\text{th}})]^2. \tag{3}$$

Such a threshold field might be due to preexisting stresses within the sample.

With this modified σ_0, the values of λ_0 predicted by Eq. (2) can be directly compared to the measured dark current spike rates r_s. Since the dependencies of the spike rates on the electric field vary among measurement series, the parameter β is fitted individually for each series, while

the values of all other constants remain as in [18]. This is in line with the fitting procedure used previously to compare r_c to measured breakdown rates, where different values of β (and no other parameter) differentiate among experimental structures, thus accounting for both geometrical differences and different levels of conditioning of the electrodes [17,18]. It is also in line with the fact that β decreases over time, due to conditioning. As seen in Fig. 7, the theoretical values of λ_0 as a function of E provide a good fit to the experimental results, with no need to further adjust the MDDF theory or any numerical values. This supports the hypothesis that the dark current spikes are, indeed, a manifestation of the fluctuations in the mobile dislocation density population as described in the MDDF model.

We note that the fit in [18] was done with $E_{\mathrm{th}} = 0$. The process of breakdown explored in [18] is controlled by the probability of exceeding the critical mobile dislocation density, which is not strongly affected by E_{th}. This is due to the different functional form of the dependence of the breakdown rate on the field [18] vs Eq. (2), and also to the fact that breakdown occurs at significantly higher fields than prebreakdown fluctuations of the dark current. In addition, it is common to include an extensive annealing stage in the manufacturing of full-scale rf accelerating structures. This leads to the reduction of internal stresses, which, in turn, are expected to result in lower E_{th}. Still, taking the threshold field into account when calculating both the current spike and breakdown rates would necessitate minor changes in the values of the fitted parameters of the MDDF model. Further investigation could determine whether a threshold field exists and affects breakdown rates in high-field pulsed rf setups such as those analyzed in [18].

C. Distribution in time

Having established that λ_0 gives a good approximation of r_s, we further assume that each observable variation of the dark current is directly related to a mobile dislocation reaching the surface of the sample. Under this assumption, the full distribution of times between current spikes can be evaluated using the MDDF model. We recall that in the MDDF model, mobile dislocations are free to move within subgrain dislocation cells [18]. Here, we need to consider the kinetics of mobile dislocations in cells adjacent to the surface, and the probability of their ejection to the surface. In general, mobile dislocations can become sessile due to either reaching the surface or collision with barriers [17,18]. However, we expect cells adjacent to the surface to be relatively denuded of the sessile dislocations which serve as barriers, due to their strong elastic interaction with the surface [27].

The process of a mobile dislocation reaching the surface involves, therefore, two steps: (i) The creation of a mobile dislocation, and (ii) the ejection of the dislocation to the surface. These are represented in the MDDF model as transitions from state n to $n+1$, followed by a transition from state $n+1$ to n. Assuming that $\mu_1 \gg \lambda_1$, as is the case in the experimental range of interest, the time between spikes can be approximated by considering the random variable $T = T_{0\to1} + T_{1\to0}$. Here, $T_{0\to1}$ and $T_{1\to0}$ are random variables describing the transition time from state $n=0$ to $n=1$ and back, respectively. Assuming, for simplicity, that each transition individually is a Poissonian process, we find that T is a two-parameter hypoexponentially distributed variable, with the rate parameters λ_0 and μ_1 [28].

We note that even though a dark current spike occurs when a mobile dislocation reaches the surface of the sample, i.e., at the transition from state $n=1$ to state $n=0$, the mobile dislocation needs to be created in order to be depleted. Since $\mu_1 \gg \lambda_0$, the average value of $T_{0\to1}$ is much greater than the average value of $T_{1\to0}$, so $E(T) \approx E(T_{0\to1})$. This is why, even though the spike of dark current corresponds to the transition $n=1\to n=0$, the *mean* time interval between spikes (used to approximate r_s) is $E(T_{0\to1}) = \lambda_0^{-1}$, as stated above.

For each voltage in each measurement series, the observed distribution of the time intervals between fluctuations was fitted to an exponential, two-parameter hypoexponential, and log-normal distribution (using MATLAB's mle function). The two-parameter hypoexponential fits yielded better results in the majority of the cases, and particularly for the higher voltages, in which there were more samples per voltage. The sum of the logarithms of the likelihood ratios [29] of all the fits was $\Sigma \ln(L_h/L_e) = 5.16\times10^5$ for the hypoexponential and exponential fits, and $\Sigma \ln(L_h/L_l) = 5.73\times10^3$ for the hypoexponential and log-normal fits. (For this calculation, the data measured at 2125 V in series B was excluded, as fitting it to any of the three distributions yielded poor results.) The quality of fit is demonstrated in Figs. 5 and 6 for three out of the 25 voltage steps in the measurement series.

V. DISCUSSION AND CONCLUSIONS

The MDDF model provides a qualitative and quantitative explanation of observed breakdown rates in high-voltage applications. The purpose of the experiment described in this manuscript was to investigate the suggestion that the fluctuations of the mobile dislocation density, which are an underlying feature of the model, can be observed before breakdown itself occurs [17,18]. Indeed, dark current spikes were discovered, and their rates match the theoretical state transition rate $\lambda_0(E)$ remarkably well, with no need to adjust the previously derived numerical parameters of the model.

The fit of the time interval distribution to a hypoexponential distribution further supports the proposal that the current spikes are an inherent feature of the dynamics described by the MDDF model. The fitted value of λ_0 can be compared to r_s. However, since $\mu_1 \gg \lambda_0$, the confidence interval for the fit of μ_1 is large, making it impractical to derive values of μ_1 as a function of the electric field.

The experiment described here was performed on ridged OFHC copper electrodes. By modifying the electrode material production process and geometry, it might be possible to vary the amount of spikes prior to breakdown. This would enable us to study the dependence of prebreakdown fluctuations on the electrode structure. A configuration in which the spike rate increases significantly would allow more data samples to be collected per measurement, allowing the estimation of μ_1, and maybe even the exploration of λ_n for $n > 0$. In addition, the current experimental setup allows the identification of strong temporal variation in the current, but not its specific shape. Thus, the current work concentrated on reproducing the distribution of times between current spikes. Future experiments can investigate the form of the emitted current within spikes, possibly providing constraints on the specific current emission mechanism.

Another subject for investigation is the value of β, in a given setup, as a function of the exposure time to electric fields. As explained in Sec. III, electrodes subject to electric fields undergo a continuous process of conditioning. As a result, while the functional form of the spike rate as a function of the electric field is consistent, the value of β [and therefore $\lambda_0(E)$] in a given setup varies over time. Until now, this variation was followed via breakdown rate measurements. The discovery of dark current spikes allows us to examine the development of β via the spike rate, without having to bring the system to breakdown. Alternatively, it might be possible to measure current spike rates and breakdown rates in the same setup, so that the values of β derived from each of them can be compared.

The observed correlation between current spikes and breakdown can be utilized to reduce the breakdown rate in high voltage setups, and improve operational procedures in such systems, by using rates of observed dark current spikes to determine the level of conditioning of electrodes, or by monitoring spikes as observed *in situ* prior to breakdown.

ACKNOWLEDGMENTS

E. Z. E., S. L., and Y. A. acknowledge funding from CERN and the PAZY foundation.

APPENDIX A: DETAILS OF THE MEASUREMENT SERIES

As stated in Sec. III, the experiment was repeated in five measurement series. Over the course of each such measurement series, the applied voltage was varied in steps over two or three cycles, so that each voltage was revisited 2 or 3 times. Each voltage step in each of the cycles consisted of eight windows, 2 s long each, between which there were intervals on the order of one minute, in which the data collected was saved to disk. An example of the voltage over the course of one measurement series is shown in Fig. 8.

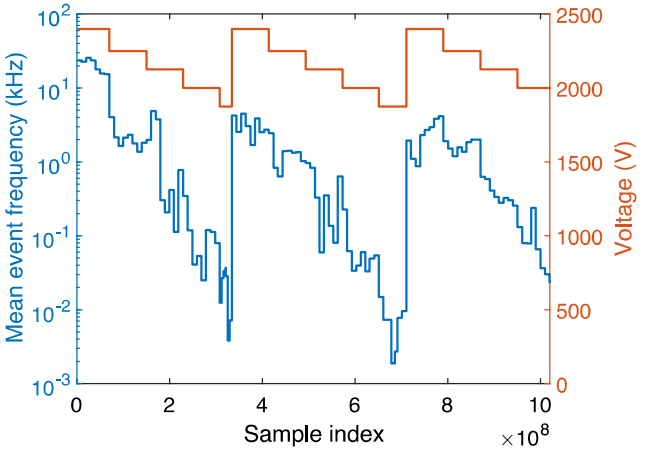

FIG. 8. Applied voltage and spike frequency over the course of measurement series C. The time in the horizontal axis is shown in units of oscilloscope samples, with the time intervals between the windows emitted.

The windows between voltage steps are omitted in the figure.

The voltages in each measurement series were chosen so as to allow the observation of as many current fluctuations

TABLE III. Details of the measurement series.

Series	Date	Voltage (V)	Electric field (MV/m)	λ_0 (10^4 s^{-1} mm^{-2})
A	10/15/2019	1875	31.3	1.34×10^{-3}
		2000	33.3	1.74×10^{-2}
		2125	35.4	8.85×10^{-2}
		2250	37.5	9.05×10^{-2}
B	10/15/2019	2125	35.4	4.69×10^{-2}
		2250	37.5	2.27×10^{-2}
		2500	41.7	1.11×10^{-1}
		2750	45.8	2.67×10^{-1}
		3000	50.0	3.64×10^{-1}
C	10/29/2019	1875	31.3	5.20×10^{-5}
		2000	33.3	6.34×10^{-4}
		2125	35.4	4.79×10^{-3}
		2250	37.5	1.97×10^{-2}
		2400	40.0	2.85×10^{-2}
D	10/31/2019	1750	29.2	9.14×10^{-5}
		1875	31.3	1.90×10^{-4}
		2000	33.3	5.24×10^{-4}
		2125	35.4	8.55×10^{-4}
		2250	37.5	1.79×10^{-3}
		2375	39.6	2.30×10^{-3}
E	11/01/2019	2000	33.3	5.78×10^{-4}
		2125	35.4	1.28×10^{-3}
		2250	37.5	2.05×10^{-3}
		2375	39.6	3.59×10^{-3}
		2400	40.0	3.01×10^{-3}

possible, while making sure that there were no breakdowns within a window. Due to these considerations, and to the effects of conditioning, the voltage steps in the different series were not identical. Table III lists the measurement series, the date at which each was carried out, the voltages in each of the series, and the applied electric field. In addition, the value of λ_0, yielding the best fit to a two-parameter hypoexponential distribution, is listed. As explained in Sec. IV, this value is also approximately equal to the rate of current spikes r_s.

APPENDIX B: SPIKE IDENTIFICATION ALGORITHM

The purpose of the spike identification algorithm was to identify the onset time of the unique current spike events. The algorithm had to distinguish the events from noise, and avoid double counting by determining whether temporally consecutive peaks of current represented separate spikes, or were caused by ringing, see Fig. 4.

Concerning the first issue, the noise in the current was assumed to be normally distributed. For a normal distribution of N samples with standard deviation σ, the expected number of samples deviating by $n\sigma$ from the mean is $F = [1 - \mathrm{erf}(n/\sqrt{2})]N$. At a sampling rate of 5 MHz and window length of 2 s, each window contains $N = 10^7$ samples. The lowest integer value of n yielding $F < 1$, i.e., less than one false positive per window on average, is, then, $n = 6$. Figure 9 shows a histogram of the absolute values of the current measured in a typical window. It is seen that the shape of the histogram diverges from a half-Gaussian beginning from a deviation between 5σ and 6σ. Therefore, at the first stage of the algorithm, the mean and standard deviation of the measured current were calculated for each window individually. Samples deviating from the mean by 6σ or more were considered as potential spike locations.

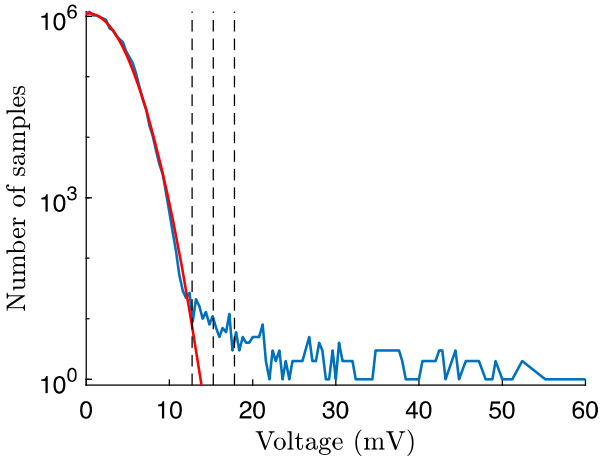

FIG. 9. Frequency histogram of the measured dark current signal values in one window, measured at an electric field of 29.2 MV/m, in measurement series D. The histogram contains 150 evenly spaced bins, each 0.4 mV (corresponding to a current of 2.3×10^7 μA) wide. The vertical dashed lines represent deviations from the mean of 5σ, 6σ, and 7σ.

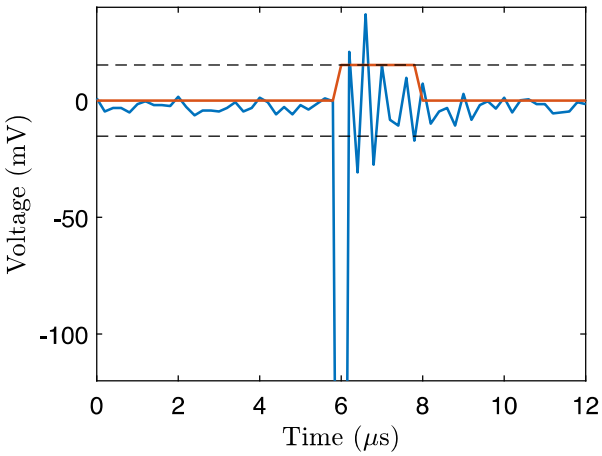

FIG. 10. Dark current signal as a function of time, shown over a period of 12 μs measured at an electric field of 29.2 MV/m in measurement series D. The first peak of the current reaches a value of approximately −800 mV. The dashed lines represent the event thresholds of 6σ, and the solid straight line shows how a number of current peaks, caused by ringing, were counted as one spike.

At the second stage, to avoid double counting due to ringing, the algorithm examined the measured current of the samples which were not discarded at the first stage. If the absolute value of the current was a maximum within a time range of ± 20 μs from the sample, it was determined to be the location of a spike. This time constant was considerably greater than the observed duration of ringing, and considerably smaller than typically observed times between spikes at all electric fields. Figure 10 shows a typical spike made up of a few peaks, each consisting of samples above the threshold of 6σ. The spike is detected by the first stage of the algorithm, and counted as exactly one spike by the second stage.

[1] *Handbook of Vacuum Arc Science and Technology: Fundamentals and Applications*, edited by R. L. Boxman, D. M. Sanders, and P. J. Martin (Noyes, Park Ridge, NJ, 1996).
[2] P. G. Slade, *The Vacuum Interrupter: Theory, Design, and Application* (CRC Press, Boca Raton, FL, 2008).
[3] *High Gradient Accelerating Structure*, edited by W. Gai (World Scientific, Singapore, 2014).
[4] G. Teel, A. Shashurin, X. Fang, and M. Keidar, Discharge ignition in the micro-cathode arc thruster, J. Appl. Phys. **121**, 023303 (2017).
[5] W. P. Dyke, J. K. Trolan, E. E. Martin, and J. P. Barbour, The field emission initiated vacuum Arc. I. Experiments on Arc initiation, Phys. Rev. **91**, 1043 (1953).

[6] S. Döbert, RF-breakdown in high-frequency accelerators, SLAC Technical Report No. SLAC-PUB-10463, 2004.

[7] P. Burrows, N. C. Lasheras, L. Linssen, M. Petrič, A. Robson, D. Schulte, E. Sicking, and S. Stapnes, The Compact Linear Collider (CLIC) 2018 summary report, CERN Technical Report No. CERN-2018-005-M, 2018.

[8] A. Descoeudres, Y. Levinsen, S. Calatroni, M. Taborelli, and W. Wuensch, Investigation of the dc vacuum breakdown mechanism, Phys. Rev. ST Accel. Beams **12**, 092001 (2009).

[9] I. Profatilova, X. Stragier, S. Calatroni, A. Kandratsyeu, E. R. Castro, and W. Wuensch, Breakdown localisation in a pulsed DC electrode system, Nucl. Instrum. Methods Phys. Res., Sect. A **953**, 163079 (2020).

[10] A. Saressalo, A. Kyritsakis, F. Djurabekova, I. Profatilova, J. Paszkiewicz, S. Calatroni, and W. Wuensch, Classification of vacuum arc breakdowns in a pulsed dc system, Phys. Rev. Accel. Beams **23**, 023101 (2020).

[11] V. Zadin, A. Pohjonen, A. Aabloo, K. Nordlund, and F. Djurabekova, Electrostatic-elastoplastic simulations of copper surface under high electric fields, Phys. Rev. ST Accel. Beams **17**, 103501 (2014).

[12] S. Vigonski, M. Veske, A. Aabloo, F. Djurabekova, and V. Zadin, Verification of a multiscale surface stress model near voids in copper under the load induced by external high electric field, Appl. Math. Comput. **267**, 476 (2015).

[13] A. Kyritsakis, M. Veske, K. Eimre, V. Zadin, and F. Djurabekova, Thermal runaway of metal nano-tips during intense electron emission, J. Phys. D **51**, 225203 (2018).

[14] W. Wuensch, Advances in the understanding of the physical processes of vacuum breakdown, CERN Technical Report No. CERN-OPEN-2014-028, 2013.

[15] A. Degiovanni, W. Wuensch, and J. G. Navarro, Comparison of the conditioning of high gradient accelerating structures, Phys. Rev. Accel. Beams **19**, 032001 (2016).

[16] A. Pohjonen, F. Djurabekova, K. Nordlund, A. Kuronen, and S. Fitzgerald, Dislocation nucleation from near surface void under static tensile stress in Cu, J. Appl. Phys. **110**, 023509 (2011).

[17] E. Z. Engelberg, Y. Ashkenazy, and M. Assaf, Stochastic Model of Breakdown Nucleation under Intense Electric Fields, Phys. Rev. Lett. **120**, 124801 (2018).

[18] E. Z. Engelberg, A. B. Yashar, Y. Ashkenazy, M. Assaf, and I. Popov, Theory of electric field breakdown nucleation due to mobile dislocations, Phys. Rev. Accel. Beams **22**, 083501 (2019).

[19] S. Calatroni, A. Descoeudres, J. W. Kovermann, M. Taborelli, H. Timko, W. Wuensch, F. Djurabekova, K. Nordlund, A. Pohjonen, and A. Kuronen, Breakdown studies for the CLIC accelerating structures, in *Proceedings of Linear Accelerator Conference (LINAC'10), Tsukuba, Japan* (JACoW, Geneva, 2010), pp. 217–219.

[20] A. Anders, *Cathodic Arcs: From Fractal Spots to Energetic Condensation*, Springer Series on Atomic, Optical, and Plasma Physics (Springer, New York, 2008), Vol. 50.

[21] A. Anders, A review comparing cathodic arcs and high power impulse magnetron sputtering (HiPIMS), Surf. Coat. Technol. **257**, 308 (2014).

[22] A. Grudiev, S. Calatroni, and W. Wuensch, New local field quantity describing the high gradient limit of accelerating structures, Phys. Rev. ST Accel. Beams **12**, 102001 (2009).

[23] A. Cahill, J. Rosenzweig, V. Dolgashev, S. Tantawi, and S. Weathersby, Ultra high gradient breakdown rates in x-band cryogenic normal conducting rf accelerating cavities, in *Proceedings of the Eighth International Particle Accelerator Conference (IPAC'17)* (JACoW, Geneva, 2017).

[24] J. Wang and G. Loew, Field emission and RF breakdown in high-gradient room-temperature linac structures, SLAC Technical Report No. SLAC-PUB-7684, 1997.

[25] P. Kranjec and L. Ruby, Test of the critical theory of electrical breakdown in vacuum, J. Vac. Sci. Technol. **4**, 94 (1967).

[26] S. V. Baryshev, S. Antipov, J. Shao, C. Jing, K. J. P. Quintero, J. Qiu, W. Liu, W. Gai, A. D. Kanareykin, and A. V. Sumant, Planar ultrananocrystalline diamond field emitter in accelerator radio frequency electron injector: Performance metrics, Appl. Phys. Lett. **105**, 203505 (2014).

[27] J. P. Hirth and J. Lothe, *Theory of Dislocations* (Krieger, Malabar, FL, 1982).

[28] D. R. Cox, *Renewal Theory* (Methuen, London, 2008).

[29] G. Bohm and G. Zech, *Introduction to Statistics and Data Analysis* (DESY, Hamburg, 2010).